

NJC

Accepted Manuscript



This article can be cited before page numbers have been issued, to do this please use: B. Chakraborty, C. Sengupta, U. Pal and S. Basu, *New J. Chem.*, 2017, DOI: 10.1039/C7NJ02454A.



This is an Accepted Manuscript, which has been through the Royal Society of Chemistry peer review process and has been accepted for publication.

Accepted Manuscripts are published online shortly after acceptance, before technical editing, formatting and proof reading. Using this free service, authors can make their results available to the community, in citable form, before we publish the edited article. We will replace this Accepted Manuscript with the edited and formatted Advance Article as soon as it is available.

You can find more information about Accepted Manuscripts in the [author guidelines](#).

Please note that technical editing may introduce minor changes to the text and/or graphics, which may alter content. The journal's standard [Terms & Conditions](#) and the ethical guidelines, outlined in our [author and reviewer resource centre](#), still apply. In no event shall the Royal Society of Chemistry be held responsible for any errors or omissions in this Accepted Manuscript or any consequences arising from the use of any information it contains.

Acridone in biological nanocavity: A detailed spectroscopic and docking analyses of probing both the tryptophan residues of bovine serum albumin

Brotati Chakraborty*¹, Chaitrali Sengupta², Uttam Pal² and Samita Basu^{2,3}

¹*Department of Chemistry, Bejoy Narayan Mahavidyalaya, Itachuna, Hooghly, West Bengal, PIN 712147, India*

²*Chemical Sciences Division, Saha Institute of Nuclear Physics, 1/AF Bidhannagar, Kolkata, West Bengal, PIN-700064, India.*

³*Homi Bhaba National Institute, Mumbai, Maharashtra, India, PIN-400094, India*

*Corresponding author:

Brotati Chakraborty, Department of Chemistry, Bejoy Narayan Mahavidyalaya, Itachuna, District: Hooghly, West Bengal, PIN 712147, India

email: brotati07@gmail.com

Abstract

Spectroscopic and docking analyses reveal that Acridone (AD) interacts with both the tryptophan (Trp) residues of Bovine Serum Albumin (BSA) (both Trp 134 and Trp 212) in contrast to other organic ligands including other acridine derivatives which generally prefer to interact with Trp 212. Use of fluorescence spectroscopy, specifically the unusual time-resolved area normalized spectra depicting two isoemissive points with different times of evolution, confirms that AD “unusually” interacts with both the Trp residues present in the model protein. Upward curvature of Stern Volmer plot suggests the interaction of AD with both the Trp residues present in varying microenvironments within BSA and possibly also indicates the denaturation of the protein. Ground state interaction of AD and BSA is explored using absorption spectroscopy, whereas strong perturbation in secondary and tertiary structures of the model protein on binding with the ligand is divulged from the observation of circular dichroism spectroscopy. Femtosecond fluorescence up-conversion kinetics implies that photoinduced electron transfer reaction takes place from the Trp residue of the protein to AD, which has been authenticated using laser flash photolysis *via* identification of the radical ions. Binding as well as thermodynamic parameters associated with AD-BSA interaction is obtained from fluorescence study. The prime deduction from the detailed spectroscopic and docking analyses is that AD initially interacts with Trp 212 present in the crevice of hydrophobic domain IIA of the protein and then perturbs the structure of BSA to bring about conformational changes such that it can gain access to Trp 134 housed in hydrophilic domain IB, which is possibly facilitated by hydrogen bonding.

Keywords: serum albumin, energy transfer, fluorescence up-conversion, electron transfer, protein microenvironment, molecular docking

1. Introduction

The study of protein-ligand interaction finds immense application in biological processes like hormone action, enzyme-substrate recognition, signal transduction and cell communication.¹ In particular, the study of binding of drugs to transport proteins like serum albumins often attracts the interest of researchers as it yields information regarding modulation of drug solubility in plasma, their susceptibility to oxidation, toxicity and *in vivo* half-life.² Investigating the behavior of probe molecules confined within nanocavities formed primarily within protein pockets is always interesting as the behavior of these trapped molecules are drastically different from those free in solution. Further, the binding ability of drug to the serum albumins may significantly influence its distribution, free concentration and metabolism. Moreover, research on drugs which can be activated by photons is more appealing since light as an activating agent is more advantageous compared to other regulating methods, especially because irradiation can be easily controlled in space and time, thus confining drug activity to selected tissues with negligible side effects.³ In this context, as photochemists our interest lies in the fact that whether photoinduced processes like energy transfer, excited state proton transfer, photoinduced electron transfer (PET) reactions etc. are taking place in systems which involve proteins and photoactivated drug molecules. Earlier we have resorted to laser flash photolysis (LFP) technique to explore PET reactions in such protein-ligand systems *via* identification and characterization of radical/radical ions pairs which are formed as primary intermediates in such reactions.^{4,5} Apart from optical spectroscopic tools like circular dichroism (CD), UV-vis absorption, FTIR, NMR etc., fluorescence spectroscopy is mainly employed to gain information regarding the binding modes of drugs with proteins. The advantage of using fluorescence spectroscopy is that the early events of molecular recognition can be directly probed by this tool because it involves the singlet state of the drug and its dynamics, which in most cases evolves on the nanosecond time scale. Steady-state fluorescence quenching, anisotropy measurements, time-resolved measurements etc. are often utilized to study drug-protein interactions.⁶⁻¹⁰ Further, femtosecond up-conversion fluorescence technique is used to investigate very fast photoinitiated processes, early time dynamics of solvated molecules soon after photoexcitation, understanding the behavior of the ligand during the early stages of photoexcitation within chemical and biological nanocavities and also to probe charge transfer reactions.¹¹⁻¹⁵

We have studied the interactions of a good number of therapeutically important molecules including some of the acridine derivatives with both the serum albumins, *viz.*, human serum albumin (HSA) and bovine serum albumin (BSA).^{4-6,16-18} We are inclined to study the photochemical properties of acridine derivatives as some of the acridine derivatives are prospective candidates of photosensitizer in photodynamic therapy.¹⁹⁻²¹ Thus, the study of interaction of these compounds in photoactivated state with biological targets may yield exciting results. Further, owing to the planar structure of acridine moiety, its derivatives can act as good intercalators, and thus the interaction of acridine compounds with nucleic acids has gained the attention of researchers.²²⁻²⁴ However, very few reports are available which discuss about the interactions of acridine derivatives with proteins. Thus, the study of interactions of acridine derivatives with model proteins like serum albumins, which are potent drug delivery vehicles is of immense pharmacological significance. Serum albumins are the most abundant carrier proteins in blood plasma which maintain the plasma colloid osmotic pressure and help in the transport of various exogeneous and endogeneous compounds such as fatty acids, drugs, metabolites etc. to the target sites. BSA is a widely studied model protein for drug delivery not only because of its homology with HSA but also because of its abundance, stability, low cost, ease of purification, unusual ligand binding properties, medical importance and wide acceptance in pharmaceutical industries.²⁵ The study of crystal structure of BSA suggests that it has a molecular mass of 66200 Da with 585 amino acids in a single polypeptide chain.²⁶ It is made up of three homologous domains (I, II and III) divided into nine loops (L1-L9) by disulphide bridges. Each domain can be subdivided into two sub-domains, A and B. BSA possesses two tryptophan (Trp) residues, *viz.*, Trp 212 and Trp 134, the initial one is located in hydrophobic binding pocket in subdomain IIA and the later is located on the surface of the albumin in domain IB. The principal binding sites of the protein are located in subdomains IIA and IIIA, which are commonly called binding sites I and II respectively.^{27,28} Results from our previous studies indicate that in most of the cases only one of the tryptophan residues of BSA (*i.e.* Trp 212) effectively interacts with the ligands similar to Trp 214 of HSA. Moreover, none of the above ligands interact with Trp 134 of BSA. Recently, we have chosen an acridine derivative, acridone (AD) (as depicted in Figure 1), which has the potential to pierce the structure of BSA probably owing to presence of a keto functional group and approach Trp 134 in domain IB of the serum albumin after interacting with Trp 212. It is relevant to mention here that recently we have

reported the photochemical interaction between AD with HSA which provides the general features of its interaction with single tryptophan.⁵ Now with this background knowledge, we make an endeavor to study the interaction of AD with BSA to find out whether it can interact with Trp 134 along with Trp 212 of the model protein using optical spectroscopic techniques like UV-vis absorption, fluorescence and CD spectroscopies and further corroborate our findings with docking studies. To the best of our knowledge, this is one of those rare reports which discuss about the use of time-resolved emission spectra (TRES) and time-resolved area normalized spectra (TRANES) to explore the photochemistry of a molecule in biological nanocavity along with the unusual appearance of two isoemissive points in TRANES at different time intervals. Time-resolved fluorescence anisotropy technique has been utilized to unravel the photo-behaviour of a drug-like molecule in presence of a model protein. The possibility of occurrence of PET involved in drug-protein interaction has been explored using femtosecond fluorescence up-conversion and LFP techniques. Further, docking studies have been carried out to substantiate our experimental findings. Thus, in the present study, apart from gaining information regarding conformational change, ground-state interaction, fluorescence quenching mechanisms, binding as well as thermodynamic parameters and possibility of PET, comparisons have been made in pertinent areas between the differential photochemical interactions of AD with HSA and BSA.

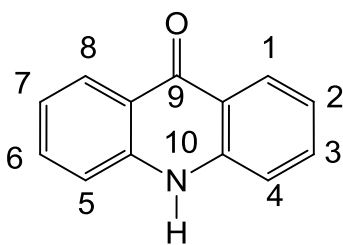


Figure 1: Chemical structure of AD

2. Experimental Methods

2.1 Materials

AD was procured from Fluka. Fatty acid- and globulin- free BSA was purchased from Sigma. Apart from the stock solution of AD, all other solutions were prepared in 10 mM phosphate buffer of pH 7.4. Stock solution of AD was prepared in UV spectroscopy grade ethanol which was procured from Spectrochem.

2.2 Apparatus

2.2.1. CD spectroscopy

CD spectra were recorded in a Chirascan spectropolarimeter (Applied Photophysics, UK) using 1 cm path length quartz cuvette. For each spectrum, three consecutive readings were averaged at a constant temperature of 298 K.

2.2.2. Absorption spectroscopy

Jasco V-650 absorption spectrophotometer was utilized for recording UV-vis absorption spectra using a pair of 1×1 cm quartz cuvettes at 298 K. Concentration of BSA was determined spectrophotometrically using the value of molar extinction coefficient of the protein at 280 nm as $43824 \text{ M}^{-1}\text{cm}^{-1}$.²⁹

2.2.3. Fluorescence Spectroscopy

Spex Fluoromax-3 spectrofluorimeter was utilized for recording steady-state fluorescence spectra using a 1×1 cm quartz cuvette at 299, 303, 308 and 314 K with excitation wavelength of 280 nm. The fluorescence of BSA was corrected for inner filter effect owing to the absorbance of AD at the excitation and emission wavelengths using the following equations:⁴

$$F_{corr} = F_{obs} \times \text{antilog} \left(\frac{OD_{ex} + OD_{em}}{2} \right) \quad (1)$$

where, F_{corr} and F_{obs} are the corrected and observed fluorescence intensities, respectively, and OD_{ex} and OD_{em} are the absorbances at excitation and emission wavelengths, respectively. Jobin Yvon Horiba picoseconds-resolved time correlated-single-photon-counting (TCSPC) spectrometer was utilized to measure fluorescence lifetime with excitation wavelength at 280 nm using pulsed diode light source Nano LED with pulse duration of 1 ns and repetition rate of 1 MHz. The data were fitted to multiexponential functions after deconvolution of the IRF by an iterative reconvolution technique using IBH DAS 6.2 data analysis software. Analysis of the fluorescence decay data $I(t)$ was done using the following equation:

$$I(t) = \sum B_i \exp\left(\frac{-t}{\tau_i}\right) \quad (2)$$

where, B_i and τ_i are the pre-exponential factors and the fluorescence lifetime, respectively. The values of χ^2 and residuals serve as the parameters for goodness of the fit. TRES and TRANES were constructed using the steady-state and time-resolved fluorescence data. Fluorescence decay measurement across the emission spectrum (290-410 nm) at particular intervals was used to construct TRES. The fitted fluorescence decays were scaled with steady-state fluorescence intensities.^{30,31} The fractional contribution of each component of the fluorescence spectrum at the wavelength of measurement was calculated using the following equation:

$$I_i(\lambda) = \frac{\alpha_i \tau_i}{\sum \alpha_i \tau_i} \quad (3)$$

where, $I_i(\lambda)$ is the fractional contribution and α_i and τ_i are the relative amplitude and lifetime of the i th component, respectively. The reconstruction of the time-resolved spectra at different time t was performed using the best fitting parameters as recommended by Maroncelli and Fleming.³² Jobin Yvon Horiba picoseconds-resolved TCSPC spectrometer was further utilized for time-resolved anisotropy decay measurements. The sample was excited at 377 nm using pulsed diode light source Nano LED with pulse duration of 100 ps and repetition rate of 1 MHz. Anisotropy $r(t)$ is defined as,³³

$$r(t) = \frac{I_{VV}(t) - GI_{VH}(t)}{I_{VV}(t) + 2GI_{VH}(t)} \quad (4)$$

where, I_{VV} and I_{VH} are the emission intensities obtained with the excitation polarizer oriented vertically and emission polarizer oriented vertically and horizontally respectively. G is the correction term for the relative throughput of each polarization through the emission optics and is given by:³⁴

$$G = \frac{I_{HV}(t)}{I_{HH}(t)} \quad (5)$$

The entire data analysis was done using IBH DAS 6.2 data analysis software to construct $r(t)$ and from the fitted curve correlation time τ_r was finally recovered.

2.2.4. Femtosecond fluorescence upconversion measurement

The fluorescence transients were measured by a femtosecond fluorescence up-conversion setup (FOG-100, CDP Corporation). The sample was excited at 400 nm with a full excitation slit width using the second harmonic of a mode-locked Ti-sapphire laser (Mai Tai, Spectra Physics), pumped by a 5 W Millennia (Spectra Physics). A nonlinear crystal (1 mm BBO, $\theta = 38^\circ$, $\phi = 90^\circ$) was used to generate the second harmonic. The fluorescence emitted from the sample was obtained under the magic angle configuration and was up-converted in another nonlinear crystal (0.5 mm BBO, $\theta = 38^\circ$, $\phi = 90^\circ$) by using the fundamental beam as a gate pulse. The up-converted light was dispersed in a monochromator and detected by photon counting electronics. The femtosecond fluorescence decays were deconvoluted using a Gaussian shape for the instrument response function having a FWHM of ~ 206 fs (obtained through water Raman scattering) using commercial software (IGOR Pro, Wave Metrics, USA). The decay traces were recorded at 460 nm. They were fitted and analyzed using IGOR Pro software to obtain fluorescence decay times.

2.2.5. Transient absorption measurement

Transient absorption spectra were measured using a nanosecond flash photolysis setup (Applied Photophysics) containing a Nd:YAG (Labseries, Model Lab150, Spectra Physics) laser. The

sample was excited at 355 nm (FWHM = 8 ns) laser light. Transients were monitored through absorption of light from a pulsed xenon lamp (150 W). The photomultiplier (R298) output was fed into an Agilent Infiniium oscilloscope (DSO8064A, 600 MHz, 4 Gs/s), and the data were transformed to a computer using the IYONIX software. The software Origin 8.0 was used for curve fitting. The solid curves were obtained by connecting the points using B-Spline option. The samples were deaerated by passing pure argon gas for 20 min prior to each experiment. No degradation of the samples was observed during the experiments.

2.2.6. Molecular docking

Molecular docking experiments were performed using AutoDock 4.2³⁵ of The Scripps Research Institute. AutoDockTools³⁵ was used for the preparation of ligands and proteins for docking. BSA (PDB: 3V03)³⁶ structural information were obtained from Protein Data Bank. The three dimensional structure of acridone was drawn in Avogadro³⁷ and geometry optimized *in vacuo* using the steepest descent followed by conjugate gradient algorithms. Molecular docking outputs were rendered in MGLTools.³⁵ Ligand interaction diagrams were generated in Schrodinger Maestro 11.0. UniProt residue numbering was used for BSA sequences (UniProtKB: P02769) where the two Trp residues are numbered as Trp 158 and Trp 237 instead of Trp 134 and 212 respectively. Solvent accessible surface area (SASA) calculations were performed at StrucTools server (<https://hpcwebapps.cit.nih.gov/structbio/basic.html>) using Mark Gerstein's calc-surface program.³⁸

3. Results and discussions

3.1. Circular dichroism spectroscopy

CD spectroscopy is a potent tool to detect the alteration in the secondary and tertiary structures of proteins. The far UV (190-250 nm) CD spectrum of native BSA shows two negative bands at 208 and 223 nm (as depicted in Figure 2A) characteristic to $\pi \rightarrow \pi^*$ and $n \rightarrow \pi^*$ transitions respectively of peptide bond, a signature of α -helical structure of proteins.^{39,40} Change in the typical characteristic α -helical structure of BSA is found on binding of AD with the serum albumin as evident from Figure 2A, implying perturbation in the secondary structure of the protein. It is observed that on addition of AD, the intensity of bands at both 208 and 223 nm is decreased. Lowering in negative ellipticity implies decrease in α -helical content of the protein.⁴¹ Figure 2A shows that the decrease in negative ellipticity is unusually more prominent at 208 nm compared to 223 nm which possibly implies that $\pi \rightarrow \pi^*$ transition of the peptide bond is more effected than $n \rightarrow \pi^*$ transition as a result of ligand-protein interaction. Also, an isodichroic point is found at 201 nm. A slight red shift of the 208 nm band is observed at lower concentration of AD while at higher concentration of AD, a new positive band at about 212 nm is formed. In fact, it is observed that at higher concentration of AD, the signature of α -helical structure of BSA is almost lost indicating a prominent perturbation in the secondary structure of BSA. It is pertinent to mention here that red shift in CD spectra indicates the possibility of hydrogen bonding in the system⁴² which will be later explored using fluorescence spectroscopy and docking technique.

Aromatic chromophores as well as the disulphide bonds present in the protein show their signatures in the near UV CD spectrum, which eventually reflects its tertiary structural organization. The characteristic wavelength profiles of the aromatic amino acid residues are as follows: tryptophan has a peak close to 290 nm, tyrosine has peaks between 275 and 282 nm while phenylalanine has sharp fine structures between 255 and 270 nm.⁴³ Moreover, near UV absorption of disulphide bonds occurs near 260 nm.⁴³ Appreciable change in near UV CD spectrum of BSA in presence of the acridine derivative (as depicted in Figure 2B) proves the perturbation in the tertiary structure of the protein. With gradual increase in concentration of AD in the solution of BSA, substantial increase in ellipticity is observed in the wavelength range of 250-265 nm which proves that binding of AD to BSA leads to conformational changes around

phenylalanine and/or disulphide bridges in the protein. It may be mentioned here that BSA contains 27 phenylalanine residues⁴⁴ and 17 disulphide bridges³⁶.

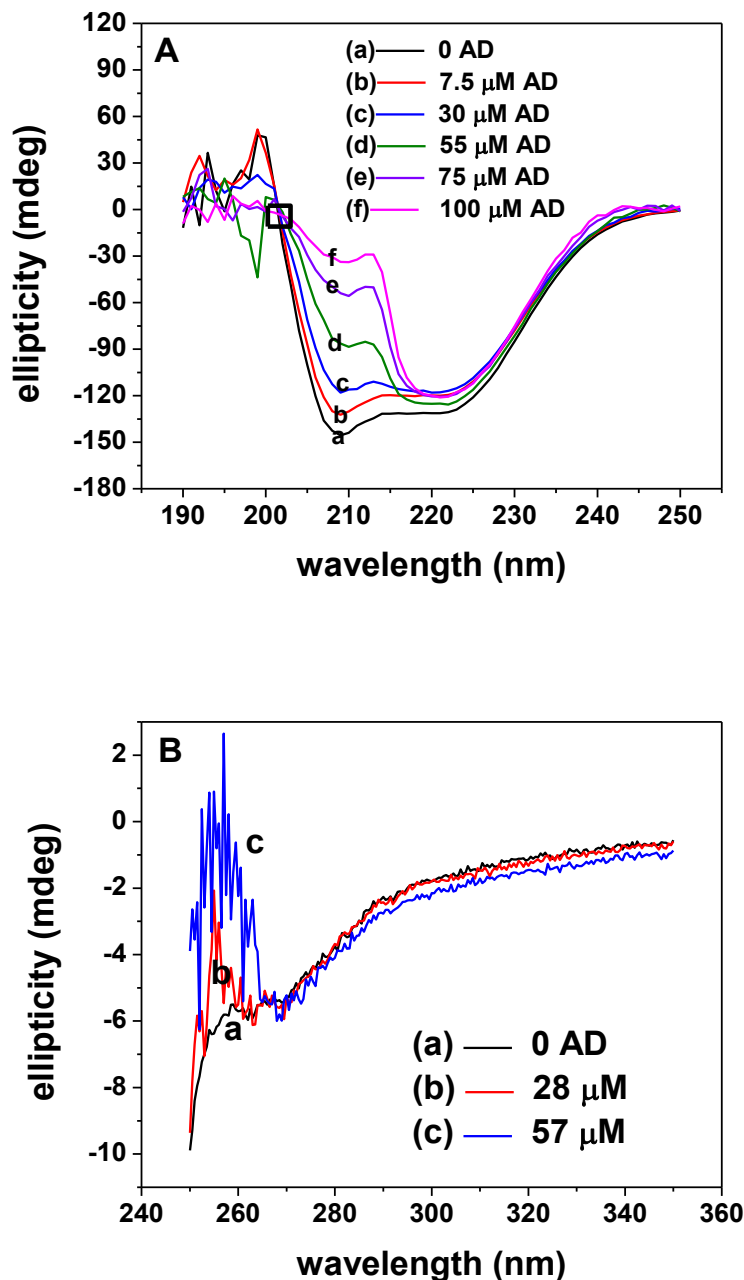


Figure 2 (A): Far UV CD spectra showing the variation of ellipticity at 208 and 223 nm on addition of AD to BSA in phosphate buffer solution of pH 7.4; [BSA] = 1 μM and [AD] varies from 0 to 100 μM . **(B)** Near UV CD spectra of BSA in phosphate buffer solution in absence and presence of AD. [BSA] = 1.5 μM and [AD] varies from 0 to 57 μM .

Thus, CD spectroscopic study reveals that both secondary and tertiary structures of BSA are perturbed in presence of BSA. It is relevant to point out here that the compounds containing keto functional groups like acetone, methyl ethyl ketone etc., have the potential to denature protein.⁴⁵ The keto group in AD may possibly be involved in causing a substantial perturbation in the secondary and tertiary structures of the model protein in the present case.

3.2. UV-vis absorption spectroscopy

Absorption spectrum of AD displays a maximum around 384 nm in phosphate buffer medium. Gradual addition of BSA to a solution of AD in phosphate buffer results in hyperchromic effect without any spectral shift as shown in Figure 3. Such an appreciable increase in absorbance at 384 nm indicates the presence of ground state interaction between AD and the serum albumin. Bardhan et. al. reported a similar enhancement in absorbance of the drug molecule on addition of BSA while studying the interaction of aurintricarboxylic acid with the serum albumin and rationalized such an observation in the light of formation of a ground state complex through inclusion of the drug molecule in the protein.⁴⁶

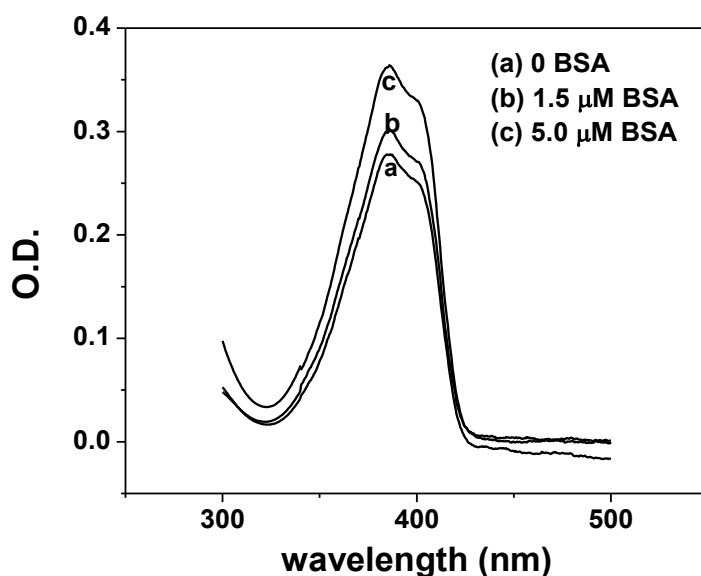


Figure 3: Absorption spectra of 40 μM AD in phosphate buffer showing hyperchromic effect on addition of BSA.

3.3. Fluorescence spectroscopy

The broad fluorescence spectrum of BSA showing maximum intensity at 348 nm is found to be quenched with addition of AD (as depicted in Figure 4), which is accompanied by enhancement in the fluorescence of AD as well as formation of an isoemissive point at 394 nm (as shown in the inset of Figure 4). Figure 4 shows that λ_{max} of the fluorescence spectrum of BSA undergoes a gradual blue shift with increase in concentration of AD indicating that the tryptophan residues in the model protein experience a hydrophobic environment in presence of AD.

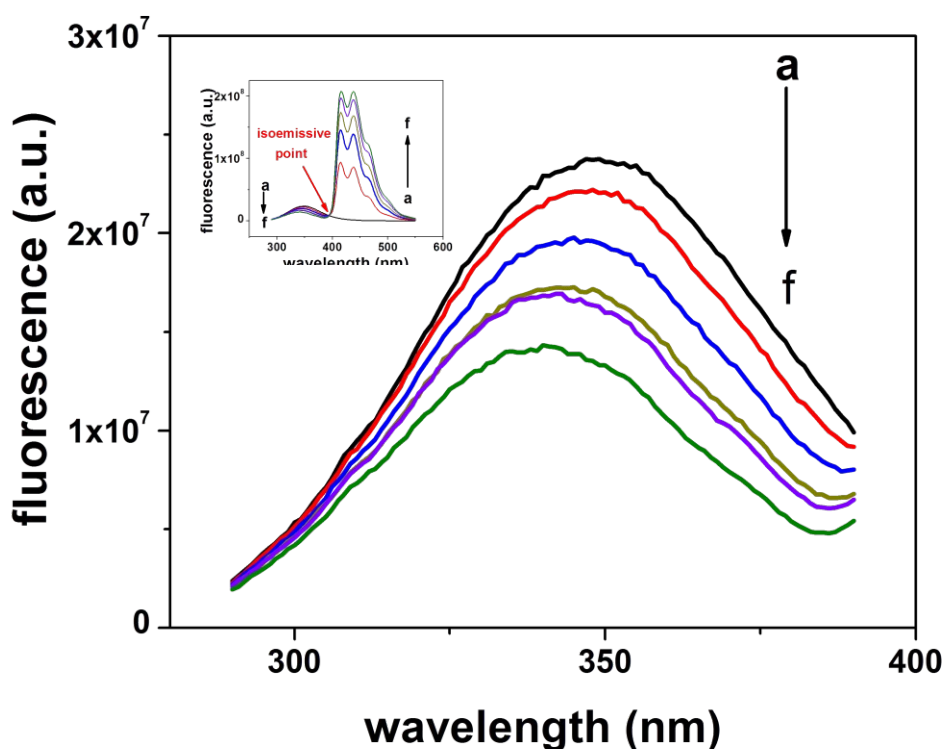


Figure 4: Fluorescence spectra showing the quenching of intrinsic fluorescence of BSA with increase in concentration of AD; $\lambda_{max} = 280$ nm. [BSA] = 1 μ M and [AD] = (a) 0, (b) 13 μ M, (c) 27 μ M, (d) 41 μ M, (e) 55 μ M, (f) 69 μ M. Inset depicts the same set of spectra in the wavelength region of 290 to 550 nm showing the isoemissive point at 394 nm.

It is customary to analyze fluorescence quenching data using Stern-Volmer (SV) equation.³⁴ Figure 5 shows that a non-linear SV plot is obtained for steady-state fluorescence quenching of the protein. In general, positive deviation from linearity of SV plot occurs when

- (a) there is a combination of static and dynamic quenching or
- (b) there is a distribution of fluorophore which interacts with the quencher, i.e. there is more than one interacting fluorophore residing in varying environments

The prevalence of static quenching mechanism is already evident from absorption spectroscopic study. In order to verify the occurrence of dynamic quenching mechanism time-resolved fluorescence study is carried out and it is found that fluorescence lifetime of BSA at 350 nm is reduced in presence of the ligand. BSA exhibits bi-exponential decay and its average lifetime (as shown in Table 1) is used to obtain a qualitative picture. Although the reduction in lifetime of BSA is very low, however, it is evident from Table 1 that with progressive increase in concentration of AD, the lifetime of BSA is lowered in a regular manner. The SV plot for time-resolved fluorescence quenching is linear (as depicted in the inset of Figure 5) as it exclusively accounts for dynamic quenching. Further, the positive deviation of SV plot may also be attributed to the presence of two tryptophan residues in BSA in varying microenvironments, one of which resides in the hydrophilic domain IB (Trp 134) on the surface of the protein and the other in hydrophobic domain IIA (Trp 212).⁴⁷ Thus, non-linearity of the SV plot is an indication of the fact that possibly both Trp 134 and Trp 212 are involved in interaction with AD. Further, Eftink and Ghiron suggested that upward curvature of SV plot may also result from denaturation of protein.⁴⁸

Considering the low concentration range of AD where SV plot for steady-state fluorescence is linear⁴⁹, the values of SV constant (K_{SV}) and quenching rate constant (k_q) are determined to be $7.38 \times 10^3 \text{ M}^{-1}$ and $1.17 \times 10^{12} \text{ M}^{-1} \text{ s}^{-1}$ respectively. The values of K_{SV} and k_q obtained from time-resolved fluorescence study are $1.06 \times 10^3 \text{ M}^{-1}$ and $1.68 \times 10^{11} \text{ M}^{-1} \text{ s}^{-1}$ respectively. Standard literature reports indicate that an order of 10^{10} is the upper limit of k_q for diffusion-controlled quenching phenomenon.³⁴ High value of k_q probably implies some photoinduced processes are occurring at faster time scale, which may give an indication of energy transfer from BSA to AD.^{50,51} Besides, the quenching of steady-state fluorescence of BSA with simultaneous increase in the emission of AD (as depicted in the inset of Figure 4) is another indication of energy transfer. Moreover, the reduction in lifetime of BSA in presence of AD is the assuring evidence of occurrence of energy transfer in the singlet state. Confirmation of the prevalence of the phenomenon of energy transfer by observing the lowering of lifetime of the donor in the

presence of acceptor has previously been reported by Patel et. al. and Barik et. al.^{49,52} The necessary condition of spectral overlap of absorption spectrum of the acceptor and the emission spectrum of the donor is satisfied by AD-BSA system as shown in Figure 6. Using the necessary equations related to energy transfer³⁴ the values of critical energy transfer distance (R_0) and distance between acceptor and donor (r) are evaluated to be 21.85 Å and 22.47 Å respectively. It is evident from the values of r and R_0 that $r < 8$ nm and $0.5 R_0 < r < 1.5 R_0$, which imply that energy transfer occurs with high probability.⁴

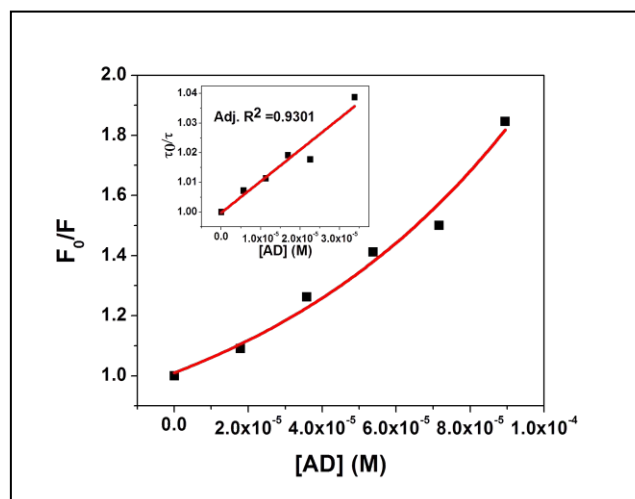


Figure 5: SV plot for quenching of steady-state fluorescence of BSA by AD; [BSA] = 1 μ M and [AD] ranges from 0 to 90 μ M. Inset shows SV plot for quenching of time-resolved fluorescence of BSA by AD; [BSA] = 1 μ M and [AD] ranges from 0 to 35 μ M.

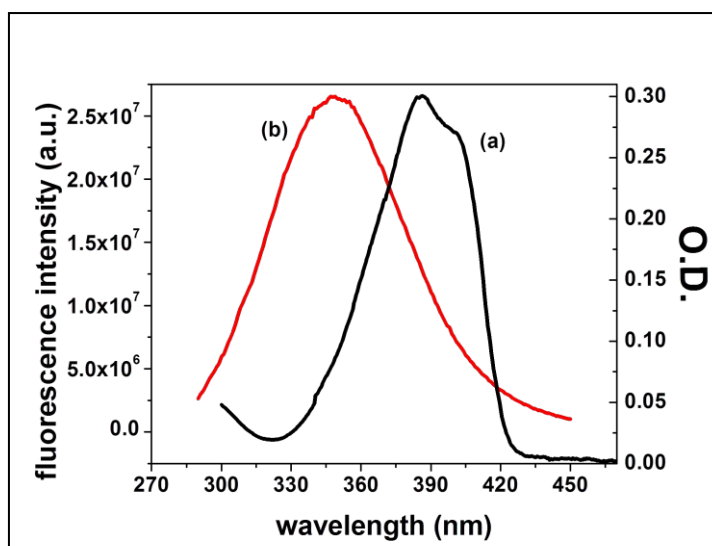


Figure 6: Spectral overlap between (a) absorption spectrum of the acceptor AD and (b) emission spectrum of the donor BSA.

Table 1: Variation of nanosecond resolved fluorescence lifetime of BSA ($\langle \tau \rangle$) with increase in concentration of AD. $\lambda_{ex} = 280$ nm and $\lambda_{em} = 350$ nm; [BSA] = 1 μ M.

[AD] (μ M)	A_1	τ_1 (ns)	A_2	τ_2 (ns)	$\langle \tau \rangle^a$ (ns)	χ^2
0	22.4	3.26×10^{-9}	77.6	6.73×10^{-9}	6.30×10^{-9}	1.06
5.64	21.41	3.10×10^{-9}	78.59	6.66×10^{-9}	6.26×10^{-9}	1.00
11.20	21.74	3.11×10^{-9}	78.26	6.64×10^{-9}	6.23×10^{-9}	0.98
16.90	19.56	2.87×10^{-9}	80.44	6.54×10^{-9}	6.19×10^{-9}	0.96
22.50	20.95	2.94×10^{-9}	79.05	6.58×10^{-9}	6.18×10^{-9}	1.04
33.80	22.02	2.87×10^{-9}	77.98	6.47×10^{-9}	6.06×10^{-9}	1.09

$$^a \langle \tau \rangle = \frac{A_1 \tau_1^2 + A_2 \tau_2^2}{A_1 \tau_1 + A_2 \tau_2}$$

Time-resolved fluorescence measurement further is carried out in order to study the photochemistry of AD in presence of BSA. It seems that the lifetime of AD remains almost unaltered with a biexponential decay profile in presence of the albumin in the nanosecond domain as shown in Table 2.

Table 2: Nanosecond resolved fluorescence lifetime of 55 μ M AD in presence of increasing concentration of BSA

[BSA] (μ M)	τ (ns)	χ^2
0	14.88	1.11
6	14.86	1.08
12	14.81	1.05
24	14.80	1.07

Thus, to gain a deeper insight into the photochemical behaviour of the acridine derivative in presence of the model protein in sub-picosecond time regime, femtosecond resolved fluorescence study has been carried out. AD shows a double exponential fluorescence decay pattern in this time regime. Upon gradual addition of protein, this fluorescence decay pattern does not change further, but the lifetime components get reduced as shown in Figure 7. This reduction in time

components (both τ_1 and τ_2) may possibly be attributed to electron transfer from tryptophan residues of BSA to AD in protein environment, which has further been explored using LFP technique in section 3.4. However, the magnitude of reduction in lifetime (as shown in Table 3) further denotes that the extent of charge transfer is very less in case of this acridone-tryptophan pair. Absence of any growth at early picosecond time regime in time resolved fluorescent transient of AD, rules out the possibility of formation of any red shifted excited state of AD in constrained environment of BSA. This observation indicates the possible residence of AD in the vicinity of tryptophan residues but in less structured water environment which could lead to slower solvation.

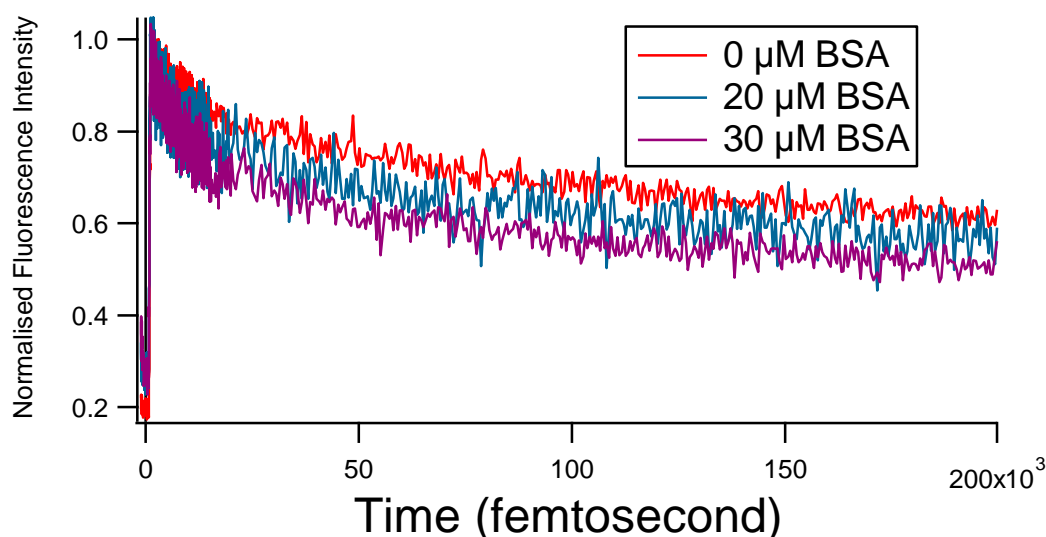


Figure 7: Femtosecond resolved fluorescence decay transients of AD (0.8mM) in presence of varying concentration of BSA. (λ_{ex} =400 nm, λ_{em} = 460 nm)

Table 3. Femtosecond resolved fluorescence decay time constants of AD (0.8mM) in presence of Varying concentration of BSA. (λ_{ex} =400 nm, λ_{em} = 460 nm)

[BSA]/ μM	τ_1 (fs)/ a_1	τ_2 (fs)/ a_2
0	11919/0.204	473708/0.795
20	7358/0.26	340763/0.73
30	9053/0.395	321340/0.605

Steady-state and time-resolved fluorescence spectra are utilized to construct TRES and TRANES. Koti and Perisamy suggested that TRANES is a more convenient method of analysis of wavelength dependent fluorescence decay compared to TRES as the former is a model free method.³⁰ TRANES analysis mainly helps to determine the number of emissive species present in the system. Figure 8A shows the TRES whereas Figures 8B and 8C show the TRANES profiles at shorter and longer time delays respectively of a solution containing both BSA and AD using $\lambda_{ex} = 280$ nm. It is evident from Figures 8B and C that two isoemissive points are obtained for AD-BSA systems at different time intervals. An isoemissive point at 328 nm is obtained within the time interval of 0-4 ns (Figure 8B) while another is observed at 390 nm in the time interval of 10-50 ns (Figure 8C). Presence of such multi isoemissive points has been reported earlier by Koti and Perisamy for multicomponent systems.³¹ In a multicomponent system, a single probe may be distributed between various regions such as, surface and interior regions of a protein or a membrane.³¹ They have experimentally shown that TRANES analysis can give two isoemissive points in different time intervals for a three component system.³¹ As stated before, in the present case, we have performed the TRES and TRANES analyses using $\lambda_{ex} = 280$ nm, implying that the tryptophan residues of BSA have been excited during the experiment.

Recently, we have reported the interaction of AD with HSA,⁵ a protein which contains only one Trp residue. Thus, in HSA there is no possibility of distribution of fluorophore. Although BSA has around 76% sequence homology with HSA,⁵³ the primary difference between HSA and BSA is that the former model protein contains only one tryptophan residue (Trp 214) while the latter contains two (Trp 212 and Trp 134). Trp 214 of HSA and Trp 212 of BSA are both located in domain IIA of the respective proteins and they experience a similar environment which is strikingly different from the environment experienced by Trp 134 of BSA located in domain IB. For HSA-AD system, the TRANES profile showed only one isoemissive point at 330 nm which was attributed to equilibrium between Trp 214 (in free HSA) and Trp 214 (in HSA) bound to AD. Thus, in AD-BSA system, the isoemissive point at 328 nm in the TRANES profile may be assigned to the equilibrium between Trp 212 (in free BSA) and Trp 212 (in BSA) bound to AD because of Trp 212 of BSA and Trp 214 of HSA are housed in similar environment in the respective proteins. Now the question that arises is what is the origin of the second isoemissive point at 390 nm in the TRANES profile with a longer time of evolution? As $\lambda_{ex} = 280$ nm is

used for the experiment, so it is obvious that the origin of the second isoemissive point also involves a Trp residue. One possibility of occurrence of the second isoemissive point is the equilibrium between Trp 134 (in free BSA) and Trp 134 (in BSA) bound to AD. However, this cannot explain the longer time of evolution because Trp 134 is more exposed to solvent compared to Trp 212 as it is located in the hydrophilic domain and is thus easily accessible to AD. Another possibility is that AD bound to Trp 212 somehow perturbs the structure of BSA and attempts to reach Trp 134. Strong perturbation in the secondary and tertiary structures of the protein at higher concentration of AD is evident from CD spectroscopic study. Thus, the second isoemissive point may also account for the equilibrium between Trp 134 (in free BSA) and Trp 134 (in BSA) bound to AD, which was previously bound to Trp 212. This also accounts for the longer time interval compared to that of the emergence of first isoemissive point. As mentioned earlier in section 3.1, compounds containing keto functional group can cause denaturation of proteins. Keto group present in AD is possibly responsible for bringing about a strong perturbation in the secondary and tertiary structures of the protein in the present case. The possibility of involvement of both the Trp residues of BSA in interaction with AD has been further explored using docking study in section 3.5.

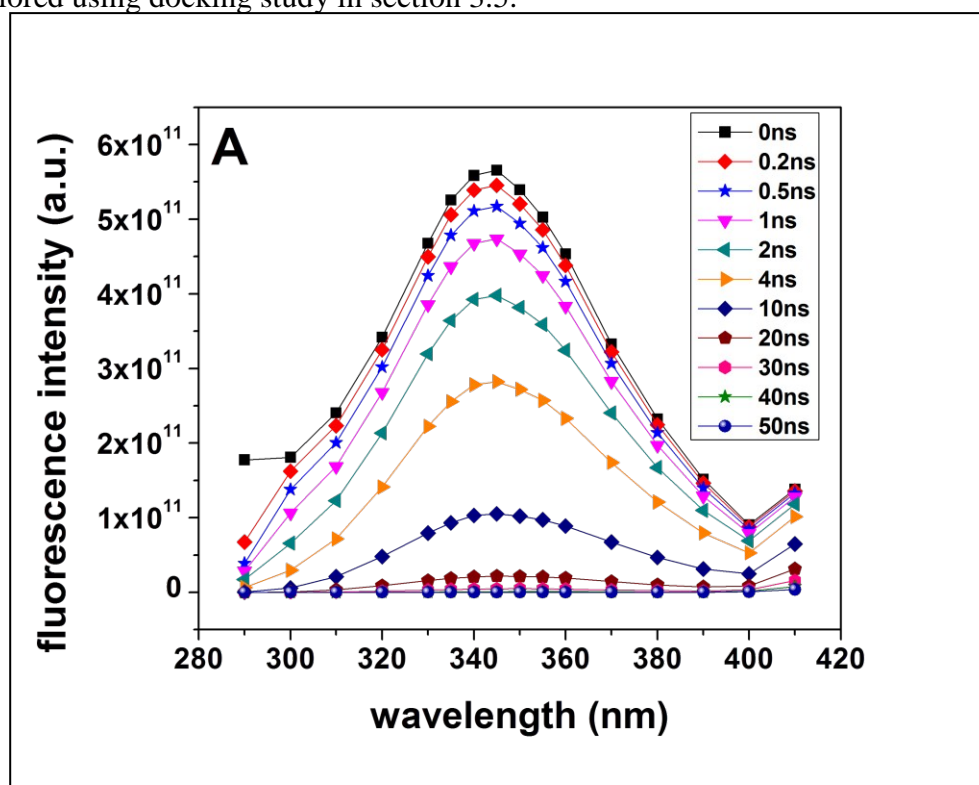


Figure 8A: TRES of AD (12.5 μM) + BSA (5 μM) in phosphate buffer solution between time 0 to 50 ns.

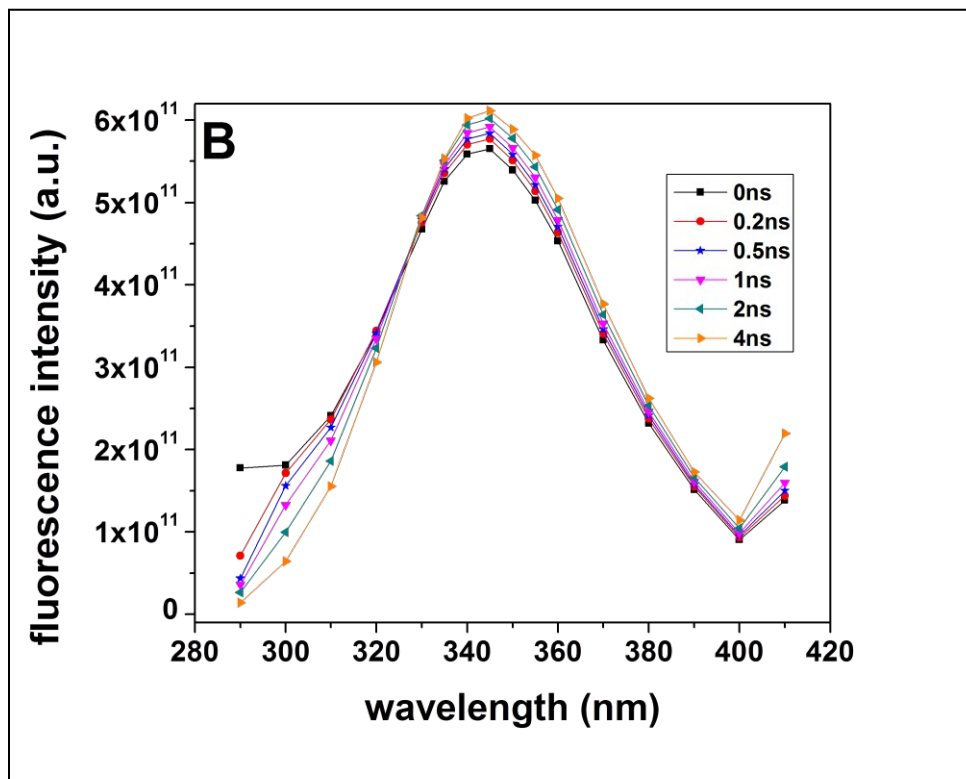


Figure 8B: TRANES of AD ($12.5 \mu\text{M}$) + BSA ($5 \mu\text{M}$) in phosphate buffer solution between time 0 to 4 ns.

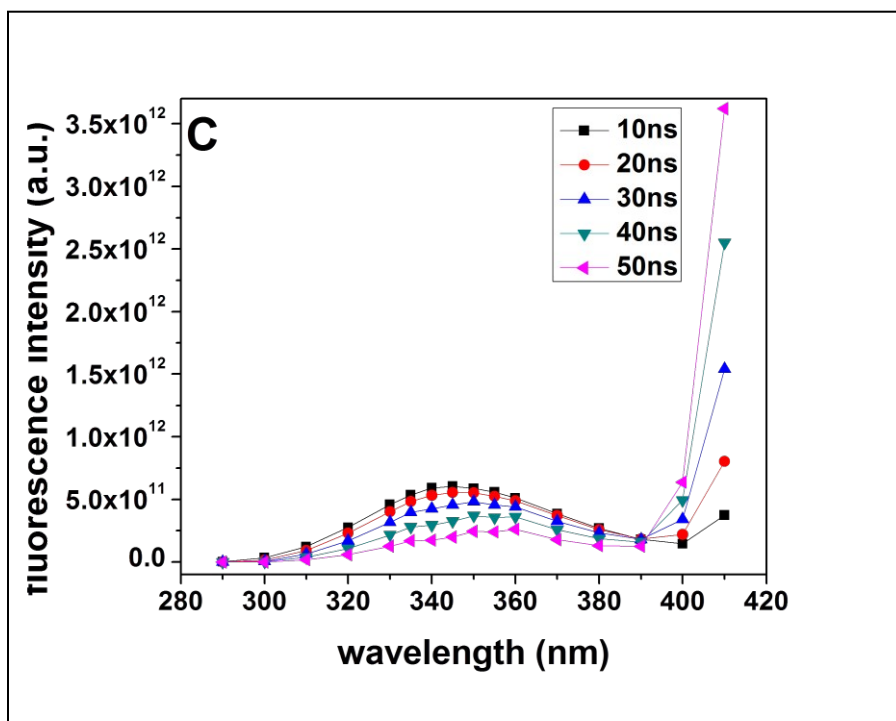


Figure 8C: TRANES of AD ($12.5 \mu\text{M}$) + BSA ($5 \mu\text{M}$) in phosphate buffer solution between time 10 to 50 ns.

As mentioned earlier in section 3.1, compounds containing keto functional group can cause denaturation of proteins. Keto group present in AD is possibly responsible for bringing about a strong perturbation in the secondary and tertiary structures of the protein in the present case as evident from CD spectroscopic studies and a possible signature of denaturation of the protein is the upward curvature of SV plot. Owing to the overall hydrophobic nature of the organic moiety, AD similar to other acridine derivatives and most of the organic ligands^{4-6,16-18,54-58} has a strong affinity to bind to vicinity of Trp 212 in domain IIA. However, due to the presence of a keto group in 9-position, AD perturbs the structure of the protein after binding to Trp 212 and brings about marked conformational changes, such that it can gain access to Trp 134 in hydrophilic domain IB. BSA loses its native conformation with increasing AD concentration, eventually making pathway for the ligand to reach Trp 134 located in domain IB. Access to hydrophilic domain is possibly facilitated by the involvement of hydrogen bonding as evident from CD fluorescence spectroscopic studies as well as docking technique. Ojha and Das reported a similar observation of a ligand initially getting hooked to one of the Trp residues of BSA to cause denaturation of the protein in order to reach the other Trp residue.⁵⁹ In fact, earlier reports suggest changes in accessibility due to conformational changes for other proteins.^{60,61}

Time-resolved anisotropy measurement is helpful in providing information about rotational motion and/or rotational relaxation of a fluorophore in a confined medium.³⁴ The anisotropy decay profiles of AD in buffer solution and in protein environment are depicted in Figures 9A and 9B respectively. For a solution containing only AD in buffer solution, the anisotropy decay fits to a single exponential function and the value of rotational correlation time is found to be 0.235 ns, whereas, for a solution containing AD in BSA the anisotropy appears to be bi-exponential with two correlation times – a shorter component of 0.184 ns (23.07%) and a longer component of 12.6 ns (76.93%). The functional form of the biexponential anisotropy decay is given by the following relation,

$$r(t) = r_0 \times \left[\alpha_{1r} \exp\left(-\frac{t}{\tau_{1r}}\right) + \alpha_{2r} \exp\left(-\frac{t}{\tau_{2r}}\right) \right] \quad (6)$$

where, r_0 is the limiting anisotropy that describes the inherent depolarization of the fluorophore and α_{ir} is the pre-exponential factor that provides the fraction of the i th rotational time, i.e., τ_{ir} . The existence of two components of correlation times obtained from the bi-exponential pattern

of anisotropy decay of AD in presence of BSA indicates the presence of two dynamic processes occurring on different time scales.^{62,63} The value of average correlation time (as shown in Table 4) apparently indicates that AD experiences a restricted environment in presence of the protein. Average correlation time is calculated using the following equation:⁶⁴

$$\langle \tau_r \rangle = \alpha_{1r} \tau_{1r} + \alpha_{2r} \tau_{2r} \quad (7)$$

Here, α_{1r} and α_{2r} are the magnitudes of the faster and slower components respectively, whereas, τ_{1r} and τ_{2r} are the observed fast and slow components respectively of the anisotropy decay. Average rotational correlation time for AD in BSA is found to be less than its fluorescence lifetime in the same, implying that depolarization is essentially complete within the excited state lifetime of the probe in the specified environment.

Several reasons may be cited regarding the origin of the biexponential behaviour of the dye in the protein environment. Firstly, the short and long components of anisotropy decay of AD in presence of BSA can be assigned to free AD and protein bound AD respectively. However, owing to the high value of binding constant of the ligand with the protein (as discussed later in this section), the validity of such a proposition may be questioned. Secondly, the biexponential nature may be rationalized in the light of rotational diffusion of AD bound to two different regions of the protein having distinctly different environments (hydrophilic and hydrophobic interaction sites of BSA) although docking study (which has been discussed elaborately in section 3.5) suggests three probable binding sites of AD on BSA. However, we feel that the observed bi-exponential decay of the fluorophore in the protein environment can be best explained in the light of ‘wobbling-in-cone’ model.⁶²⁻⁶⁸ Study of literature suggests that such bi-exponential decay may be interpreted in terms of occurrence of different kinds of rotational motions of the probe in protein environment.⁶²⁻⁶⁶ According to this model the fluorescence anisotropy decay is a product of three independent motions:

- (i) wobbling of the probe $r_W(t)$ with a time constant τ_W ,
- (ii) translation of the probe $r_D(t)$, along the surface of the protein, with a time constant τ_D , and
- (iii) overall rotation $r_P(t)$ of the protein with a time constant τ_P .

Thus, $r(t)$ may be decomposed as a product of three independent motions as,

$$r(t) = r_W(t)r_D(t)r_P(t) \quad (8)$$

Again, $r(t)$ maybe expressed in terms of the generalized order parameter S as,

$$r(t) = r_0 \left[S^2 + (1 - S^2) \exp\left(-\frac{t}{\tau_W}\right) \right] \exp\left[-t\left(\frac{1}{\tau_D} + \frac{1}{\tau_P}\right)\right] \quad (9)$$

In the wobbling-in-cone model, S is related to the semi-cone angle θ as follows:^{62,65}

$$S = 0.5 \cos\theta(1 + \cos\theta) \quad (10)$$

The order parameter S is a measure of the spatial restriction having values between 0 (corresponding to unrestricted motion) to 1 (for complete restriction on the motion).

Comparing equation (8) and (9) the following relations are obtained:

$$S^2 = \alpha_{2r} \quad (11)$$

$$\frac{1}{\tau_{2r}} = \frac{1}{\tau_D} + \frac{1}{\tau_P} \quad (12)$$

$$\frac{1}{\tau_{1r}} = \frac{1}{\tau_W} + \frac{1}{\tau_{2r}} \quad (13)$$

The wobbling-in-cone diffusion co-efficient D_W is given by the following equation for $\theta \leq 30^\circ$:

$$D_W = \frac{7\theta^2}{24\tau_W} \quad (14)$$

whereas, for $\theta \geq 30^\circ$ D_W is represented as follows:

$$D_W = \{(1 - S^2)\tau_W\}^{-1} \left[\frac{x^2(1+x)^2}{2(x-1)} \left\{ \ln\left(\frac{1+x}{2}\right) + \left(\frac{1-x}{2}\right) \right\} + \left(\frac{1-x}{24}\right) (6 + 8x - x^2 - 12x^3 - 7x^4) \right] \quad (15)$$

where, $x = \cos \theta$.

Equation (14) has been used to calculate the value of D_W as $\theta < 30^\circ$ in the present case.

The calculated parameters associated with the wobbling motion of the drug within the protein are compiled in Table 4.

Table 4: Rotational parameters of AD in aqueous buffer phase and in presence of BSA.

environment	τ_{1r} (ns)	τ_{2r} (ns)	α_{1r} (%)	α_{2r} (%)	$\langle \tau_r \rangle$ (ns)	S	θ (degree)	τ_w (ns)	$D_w \times 10^{-8}$ (s^{-1})
aq. buffer	0.235	-	100	-	0.235	-	-	-	-
BSA	0.184	12.6	23.07	76.93	9.73	0.877	23.79	0.187	2.68

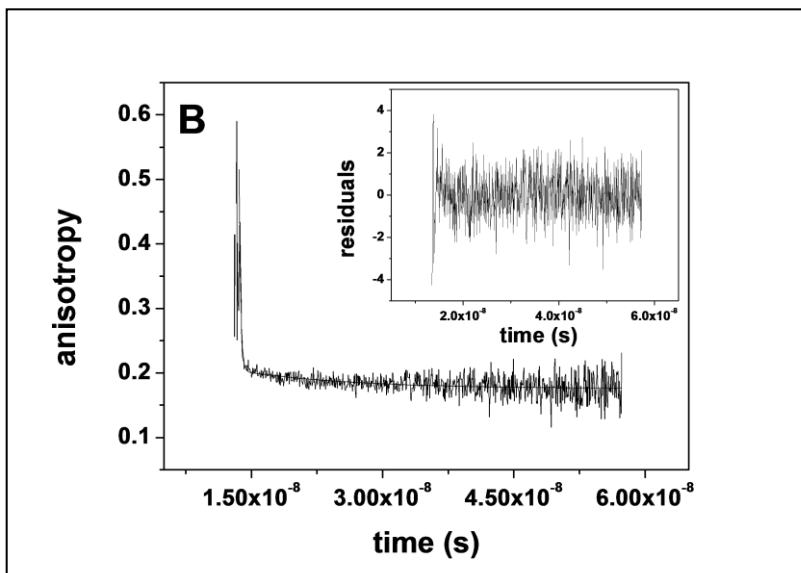
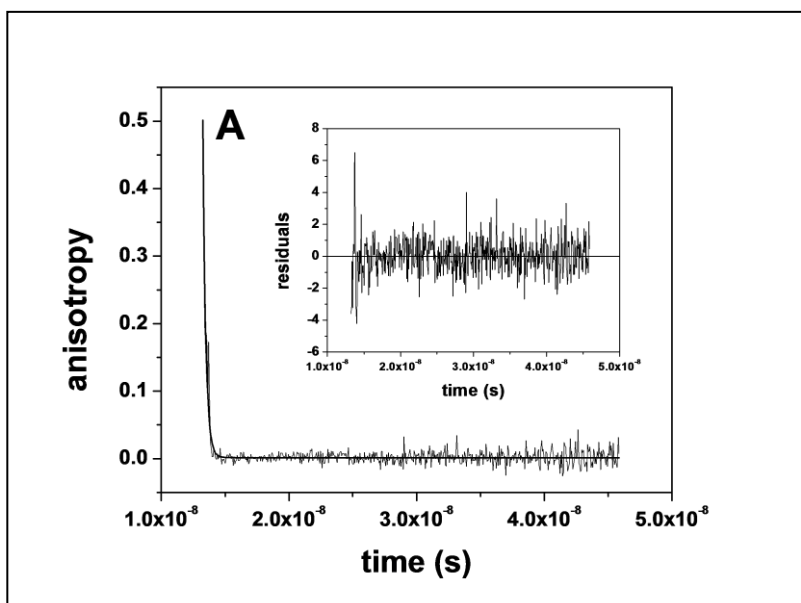


Figure 9: Time-resolved anisotropy decay curves for (A) a solution of 6 μM AD and (B) a solution containing 6 μM AD + 20 μM BSA; $\lambda_{\text{ex}} = 377 \text{ nm}$ and $\lambda_{\text{em}} = 420 \text{ nm}$.

Paul et. al. and Sahu et. al. reported the value of τ_p for BSA.^{62,66} The values of τ_p obtained by these groups suggests that $\tau_p \gg \tau_{2r}$ which possibly indicates that τ_D principally contributed to τ_{2r} which in turn implies that translational motion of the probe along the surface of the protein plays a major role in the anisotropy decay of the probe.

Quantitative estimation of binding constant (K) and binding site numbers (n) based on analysis of fluorescence quenching data can be done using the following equation:^{69,42}

$$\log\left(\frac{F - F_0}{F}\right) = \log K + n \log[Q] \quad (16)$$

where, F_0 and F are the fluorescence intensities in the absence and presence of quencher, and $[Q]$ is the concentration of quencher. From intercept and slope of the plot of $\log(F - F_0)/F$ versus $\log[Q]$, the values of K and n respectively are obtained. Also, the fluorescence quenching study at various experimental temperatures helps in assessing the thermodynamic parameters such as ΔG° , ΔH° and ΔS° associated with AD-BSA interaction. Assuming that the value of ΔH° remains almost unaltered within the range of experimental temperature, van't Hoff and Gibbs-Helmholtz equations are used to evaluate the thermodynamic parameters.

$$\ln K = -\left(\frac{\Delta H^\circ}{RT}\right) + \left(\frac{\Delta S^\circ}{R}\right) \quad (17)$$

$$\text{and } \Delta G^\circ = \Delta H^\circ - T\Delta S^\circ \quad (18)$$

ΔH° and ΔS° are obtained respectively from slope and intercept of the plot of $\ln K$ versus $1/T$. ΔG° at different temperatures are evaluated using the equation (18). Table 5 summarizes the values of binding and thermodynamic parameters at various temperatures using the results obtained from the analysis of fluorescence quenching data.

The signs of the thermodynamic parameters are often used to determine the nature of forces involved in drug-protein interaction. The model of interaction on the basis of thermodynamic parameters as suggested by Ross and Subramanian is as follows:⁷⁰

- (i) $\Delta H > 0$, $\Delta S > 0$ correspond to hydrophobic forces

- (ii) $\Delta H < 0$, $\Delta S < 0$ correspond to van der Waals interaction, hydrogen bond formation
- (iii) $\Delta H < 0$, $\Delta S > 0$ correspond to electrostatic interaction

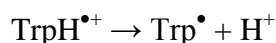
Table 5: Values of binding and thermodynamic parameters for AD-BSA system at different temperatures.

Temperature (K)	n	K (M ⁻¹)	ΔG° (kJ mol ⁻¹)	ΔH° (kJ mol ⁻¹)	ΔS° (J mol ⁻¹ K ⁻¹)
299	1.31	1.59×10^5	-29.26	-68.79	-132.2
303	1.23	6.66×10^4	-28.73		
308	1.21	5.96×10^4	-28.07		
314	1.15	3.68×10^4	-27.28		

Table 5 suggests the exothermicity of the reaction (ΔH° is negative) with an overall negative Gibb's free energy change indicating the spontaneity of AD-BSA interaction. It is observed that the value of K decreases with rise in temperature possibly implying the formation of a complex between AD and BSA which loses its stability at higher temperature. Further, negative values of ΔH° and ΔS° suggest the predominance of van der Waals interaction and hydrogen bonding in the binding interaction. An indication of involvement of hydrogen bonding in the system has already been obtained from circular dichroism spectroscopic study. It may be mentioned here that the value of binding constant of AD with BSA (as depicted in Table 5) is slightly lower in comparison with its binding constant with HSA,⁵ probably because of the dynamic nature of AD within BSA to approach both the Trp residues in varying micro environments of the protein at different time scales, whereas in AD-HSA system, the ligand specifically has an affinity for the sole Trp residue. It must be mentioned here that BSA has a more rigid structure compared to that of HSA in solution phase.⁷¹ However, the rigidity in the structure of the protein is lost on interaction with AD, thus allowing AD to move from Trp 212 to Trp 134.

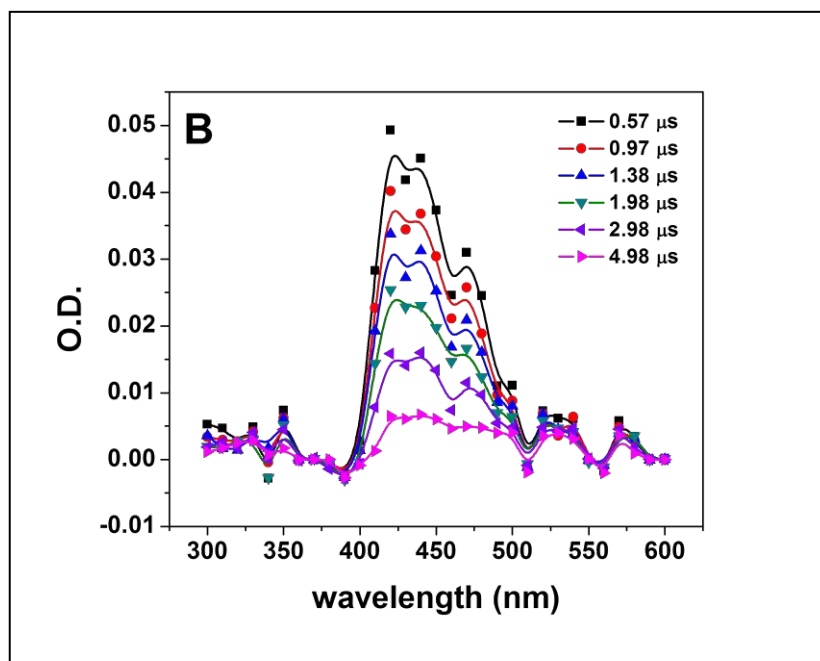
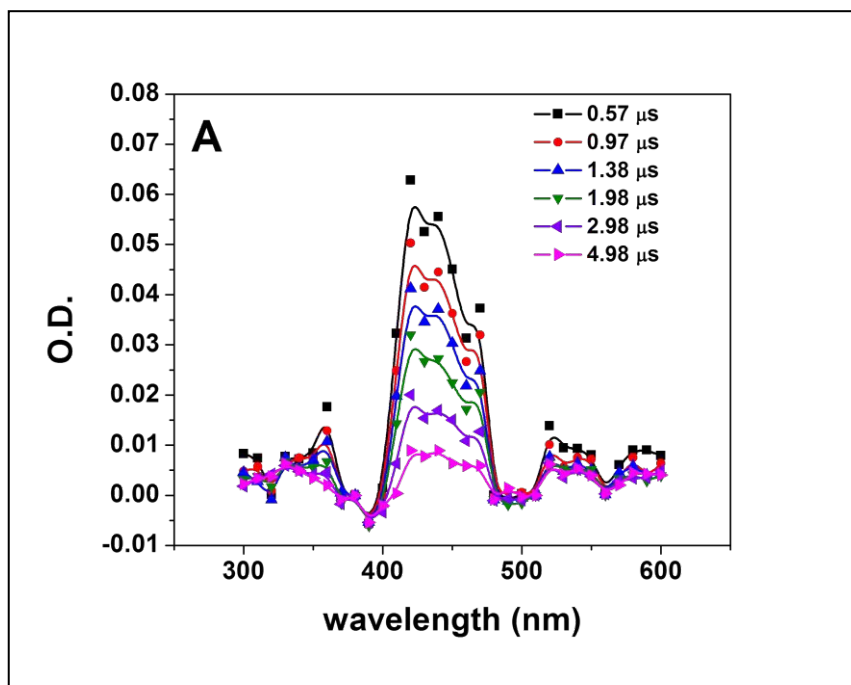
3.4. Laser Flash Photolysis

LFP is used to substantiate the findings of femto-second resolved fluorescence study which has already given an indication of occurrence of charge transfer in excited state from AD to BSA. The radical ion pairs formed during electron transfer can be detected using LFP technique which in turn may be used to confirm PET. Previous studies suggest that the transient absorption spectral signatures of $\text{TrpH}^{\bullet+}$ are found at 350 nm⁷² as well as 560 nm⁷³ and that of Trp^{\bullet} is at 510 nm⁷⁴. Further, our group has already reported that triplet–triplet transient absorption spectrum of AD has a broad peak in the wavelength region spanning from 400 to about 500 nm with a maximum at 430 nm along with a small peak around 350 nm and the characteristic peak of $\text{AD}^{\bullet-}$ appears around 510 nm.⁷⁵ Figures 10 A and B show the transient absorption spectra of 20 μM AD at 0.57, 0.97, 1.38, 1.98, 2.98 and 4.98 μs time delays after the triggering of the laser pulse in absence and presence of BSA respectively. Figure 10A shows that the spectral signatures of $^3\text{AD}^*$ at 360 and 420 nm are stable at longer time delay. On comparing figures 10 A and B it is evident that the spectral features of $^3\text{AD}^*$ undergoes a marked change on addition of BSA. Figure 10C shows that on adding protein to a solution of AD, the characteristic peaks of $^3\text{AD}^*$ at 360 and 420 nm are quenched accompanied by increase in absorbance in the wavelength region of 470-510 nm. Das and Nath studied the interaction of thioxanthone with tryptophan⁷⁶ and observed the formation of a broad band at 460-520 nm which they assigned to Trp^{\bullet} although the characteristic peak of the amino acid radical is known to appear around 510 nm. Moreover, as mentioned earlier, the characteristic peak of $\text{AD}^{\bullet-}$ appears around 510 nm. Thus, enhancement in absorbance in the wavelength region of 470-510 nm may originate from simultaneous formation of $\text{AD}^{\bullet-}$ and Trp^{\bullet} . Formation of $\text{AD}^{\bullet-}$ may take place as a result of PET from the tryptophan residue of BSA to AD. However, if PET takes place from Trp residue of the protein to the acridine derivative then $\text{TrpH}^{\bullet+}$ should also be formed. Now, the pertinent question that arises here is that why no spectral signature of $\text{TrpH}^{\bullet+}$ is observed in Figure 10C? The plausible reason for such an observation may be that deprotonation of the radical cation of tryptophan ($\text{TrpH}^{\bullet+}$) to form the corresponding radical (Trp^{\bullet}) is a well-established reaction pathway.^{72,77,78}



Thus, figure 10C may be rationalized in the light of PET taking place from tryptophan residue of the protein to AD which leads to the formation of $\text{AD}^{\bullet-}$ as well as $\text{TrpH}^{\bullet+}$ and the radical cation

of tryptophan subsequently forms Trp^\bullet *via* deprotonation. The decay profiles of 20 μM AD in presence and absence of BSA at 490 nm are depicted in Figure 10D which shows the enhancement in the yield of $\text{AD}^{\bullet-}$ and Trp^\bullet when the protein is added to a solution of AD.



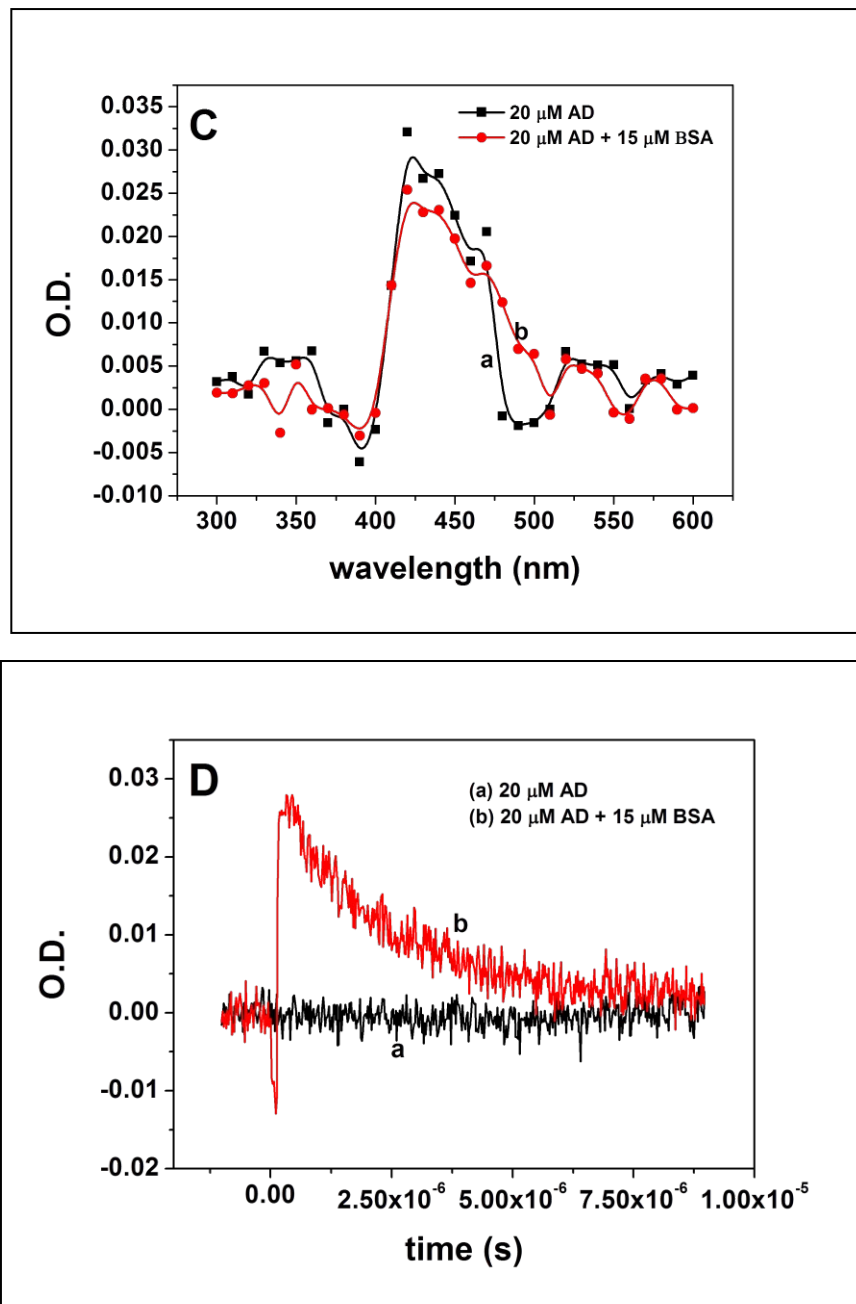


Figure 10 (A): Time resolved transient absorption spectra of 20 μM AD at 0.57 (\blacksquare), 0.97 (\bullet), 1.38 (\blacktriangle), 1.98 (\blacktriangledown), 2.98 (\blacktriangleleft) and 4.98 (\blacktriangleright) μs after the laser flash at 355 nm. (B) Time resolved transient absorption spectra of 20 μM AD in presence of 15 μM BSA at 0.57 (\blacksquare), 0.97 (\bullet), 1.38 (\blacktriangle), 1.98 (\blacktriangledown), 2.98 (\blacktriangleleft) and 4.98 (\blacktriangleright) μs

after the laser flash at 355 nm. (C) Transient spectra of (a) 20 μM AD (■) and (b) 20 μM AD in presence of 15 μM BSA (●) in phosphate buffer of pH 7.4 at 1.98 μs after the laser flash at 355 nm. (D) Decay profiles of (a) 20 μM AD (b) 20 μM AD in presence of 15 μM BSA in phosphate buffer of pH 7.4 at 490 nm after laser flash at 355 nm.

A pertinent issue in this context is the use of a weak magnetic field (MF) to determine the initial spin state of the precursors of PET.^{4,5} MF effect is primarily governed by the distance between the geminate radical ion pairs formed in the due course of PET and is substantially obtained when the separation distance is between 10-20 \AA . In case of AD-HSA system substantial MF effect is observed⁵ while in case of AD-BSA system no such MF effect is found although PET occurs in both the systems. Actually in AD-HSA system, AD specifically interacts with the sole Trp residue and AD trapped in the crevice of domain IIA of HSA strategically maintains the optimum distance from the tryptophan residue required for observation of MF effect. On the other hand, in AD-BSA system, AD initially interacts with the Trp residue housed in domain II and then perturbs the rigid structure of the protein to approach the Trp residue of domain I as suggested by TRANES profile. This dynamic behavior of AD within the protein is an unfavorable factor in the issue of preserving the optimum separation distance between the primary geminate radical ion pairs required to make exchange interaction negligible for observing substantial MF effect.

3.5 Docking study

In silico molecular docking calculation shows that the interactions of AD with the serum albumin is thermodynamically favorable with binding energy of $-31.67 \text{ kJ mol}^{-1}$ which is very close to that of the experimentally obtained value. Further, molecular docking has provided insight into the most favorable binding site for AD on BSA. As mentioned earlier in Section 2.2.6, according to UniProt numbering the two Trp residues of BSA are numbered as Trp 158 and Trp 237 instead of Trp 134 and Trp 212 respectively. In order to obtain a statistically significant result, genetic algorithm is run for 100 times and the results are clustered according to the spatial distributions and binding energy. Three major clusters are obtained, which suggests three probable binding sites of AD on BSA (Figure 11). The lowest energy cluster obtained by AutoDock 4.2 shows that the binding sites for AD lies in the groove of domain II of BSA (Figure 11). Two other binding sites were obtained in domain III and domain I, respectively. Study of literature suggests that

multiple ligand binding is a common phenomenon for serum albumins.⁷⁹⁻⁸¹ Therefore, we have probed all the three significant binding modes obtained by docking simulations. We have calculated the distances of the ligand in all three binding modes from the two Trp residues of BSA. Distances from the centres of mass of AD to the centre of mass of the amino acid residues are calculated and enlisted in table 6.

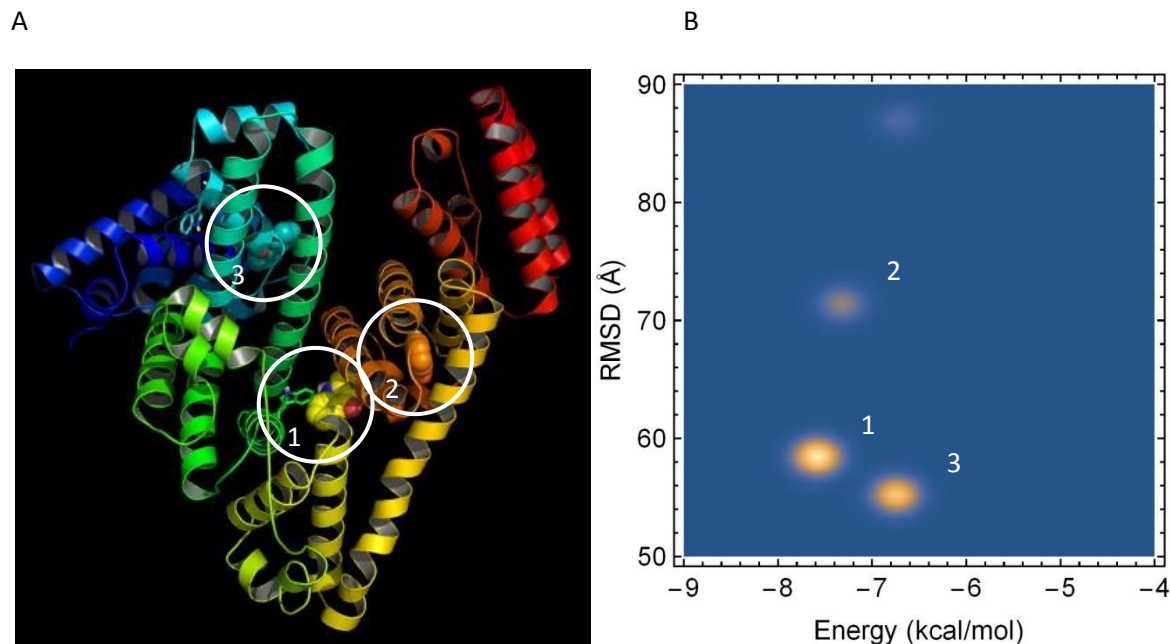


Figure 11: Interaction of AD with BSA as obtained by AutoDock 4.2. (A) Most probable binding sites of AD on BSA. (B) Probability densities of the interaction at different site and the binding energies. Binding at site 2 is less probable although energetically more favorable than binding at site 3. Conformation 1 (energetically most favorable and statistically most probable) is near to Trp 237 in domain II of BSA. Conformation 3 (energetically less favorable but statistically significant) is near Trp 158 in the domain I of BSA.

Table 6: Distances of the centre of mass of AD from the two tryptophan residues.

	Trp 158	Trp 237
Binding mode 1	33.24 Å	8.05 Å
Binding mode 2	36.45 Å	19.51 Å
Binding mode 3	23.65 Å	28.88 Å

TRANES profiles (in section 3.3) experimentally establishes the involvement of both the Trp residues of BSA in interaction with AD, which is further evident from Figure 11B depicting that conformation1 involving Trp in domain II is energetically most favourable and statistically most probable while conformation 3 involving Trp in domain I is energetically less favourable but statistically significant.

Detailed interaction diagrams of the protein–ligand complex showing the interacting residues and the types of interactions obtained by molecular modeling are given in Figure 12. Best binding conformation of AD is found to be in the groove II of BSA. Leu221, Trp237, Leu370, Leu476, Leu480, Leu504 and Val505 provide the hydrophobic environment for binding. Polar amino acids Ser367, Ser477, Asn481 and charged amino acids Arg371, Arg507 and Arg508 also interact with AD. The Arg371 residue is found to form hydrogen bonding interaction with AD. Moreover, Trp237 is found to form a pi-stacking interaction with AD. Details of the interacting residues at two other probable binding sites are highlighted in Figure 12. Binding to these two sites are energetically less favourable, however, statistically significant. Hydrophobic interactions, hydrogen bonding, pi-pi/cation interactions are the major forces governing the interactions at all three sites. The possibility of involvement of hydrogen bond interaction has already been obtained from CD and fluorescence spectroscopic studies and is further corroborated by docking study. Hydrogen bonding distances for all the three conformations are listed in Table 7. Presence of hydrogen bonding suggests a decrease in hydrophilicity which substantiates the blue shifting of λ_{em} of tryptophan emission spectra in presence of AD.⁴²

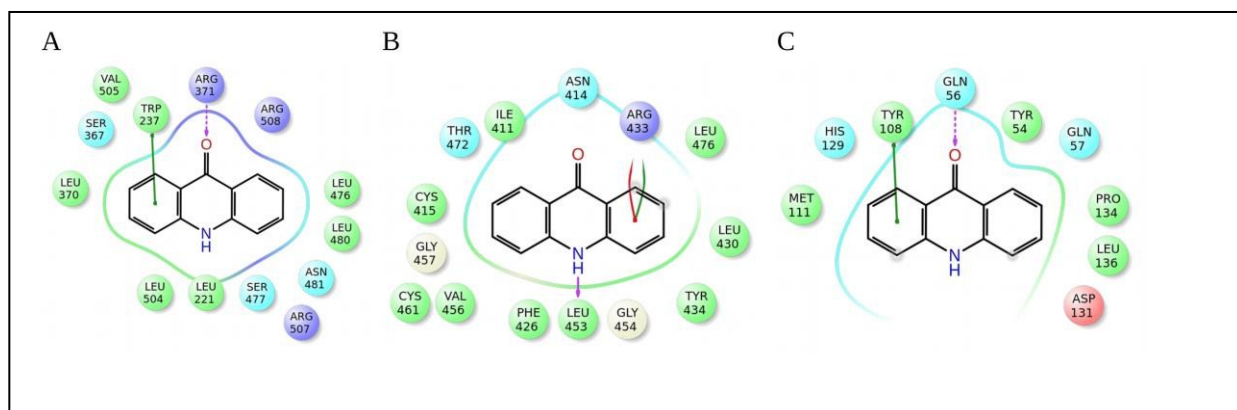


Figure 12: Interacting residues at the three most probable binding sites. Detailed interaction diagram of AD with BSA as obtained by molecular docking experiments. A,B,C correspond to conformations 1, 2 and 3 respectively. Green indicates hydrophobic residues; positive and negatively charged residues are shown in purple and red respectively.

Table 7: Hydrogen bonding distances of atoms of AD from various atoms of the residues of BSA

	Atoms of AD	Atoms of residues of BSA	Distance (Å)
Conformation 1	O of AD	H attached to N _η of Arg 371	2.31
Conformation 2	H attached to N of AD	O of Leu 453	2.17
Conformation 3	O of AD	H attached to C _α -N of Gln 56	2.19

Solvent accessible surface area which is abbreviated as SASA, is an index of forming contacts between the atoms on the surface of a protein and the solvent (water) molecules. Molecular docking does not directly give the solvent effects in ligand protein interactions. However, effect of solvent exclusion can be derived from the docking experiments by probing the changes in the SASA of protein residues and the ligand. Prior to interaction, the surface area of the ligand was 362.97 Å² and the surface area of BSA was 27292.13 Å². Upon complex formation the accessible surface of BSA was reduced by 87.69, 147.46 and 152.45 Å² for the three binding modes, respectively. On the other hand the ligand surface area was reduced to 1.89, 4.54 and 57.37 Å² in the three binding modes, respectively. It suggests that, in conformations 1 and 2 the ligand gets completely internalized into the BSA, whereas in conformation 3 it is slightly solvent exposed. The extent of changes in the solvent accessible surface area for the amino acid residues of BSA are also calculated and shown graphically in the figure 13. Remarkable change in the SASA is observed for residues Gln57, Tyr108, His129, Asp131, Pro134, Asn414, Tyr434, Leu453, Leu476, Ser477 and Leu504 as depicted in figure 13.

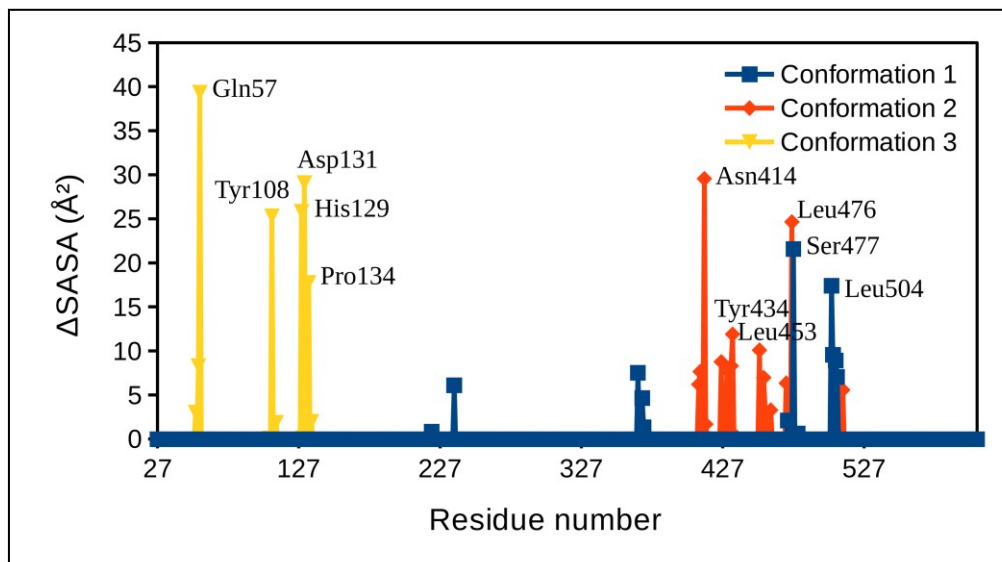


Figure 13: Changes in the solvent accessible surface area (SASA) of the interacting residues of BSA at the three most probable binding sites.

4. Conclusion

The mechanism of binding of AD to BSA is investigated using UV-vis absorption, circular dichroism, steady-state as well as time-resolved fluorescence spectroscopic tools and flash photolysis technique along with docking study. AD and BSA show ground state interaction as evident from absorption spectroscopic study. CD spectroscopy reveals strong perturbation in the secondary as well as tertiary structures of BSA in presence of AD and gives an indication of involvement of hydrogen bonding. Fluorescence quenching helps to determine the values of binding constant ($1.59 \times 10^5 \text{ M}^{-1}$ at 299 K), number of binding site (1.31 at 299 K) and the thermodynamic parameters associated with the interaction. Negative values of ΔH° ($-68.79 \text{ kJ mol}^{-1}$) and ΔS° ($-132.2 \text{ J mol}^{-1} \text{ K}^{-1}$) imply the involvement of van der Waals interaction and hydrogen bonding in the binding interaction. Upward curvature of SV plot gives an indication of occurrence of both static and dynamic quenching, interaction of AD with both the Trp residues (Trp 134 and Trp 212) present in varying environments within BSA and denaturation of the protein. Energy transfer in the singlet state occurs in AD-BSA system, which is confirmed from

fluorescence lifetime measurement. A detailed time-resolved anisotropy study is carried out and the rotational parameters of AD in absence and presence of BSA are calculated which are explained in the light of 'wobbling-in-cone' model. To take a deeper insight into the binding mechanism of AD with BSA, TRES and TRANES analyses are carried out, which are quite rare in case of drug-protein interaction. Unusual TRANES with two isoemissive points with different times of evolution strongly points towards the interaction of AD with both the Trp residues of BSA. Fluorescence upconversion and flash photolysis techniques authenticate the occurrence of PET from the Trp residues of the model protein to AD. Docking analysis suggest the involvement of Trp 134 and 212 in the interaction of BSA with AD. Integration of the results obtained from spectroscopic and docking analyses suggest that AD initially gets hooked to Trp 212 housed in domain IIA, inducing strong conformational changes in the protein probably due to the presence of keto group in the 9-position, paving way for the ligand to reach Trp 134 located in domain IB.

Conflict of interest

There are no conflicts of interest to declare.

Acknowledgement

Financial support from the Biomolecular Assembly, Recognition and Dynamics (BARD) project of Saha Institute of Nuclear Physics, Department of Atomic Energy, Government of India is greatly acknowledged.

References:

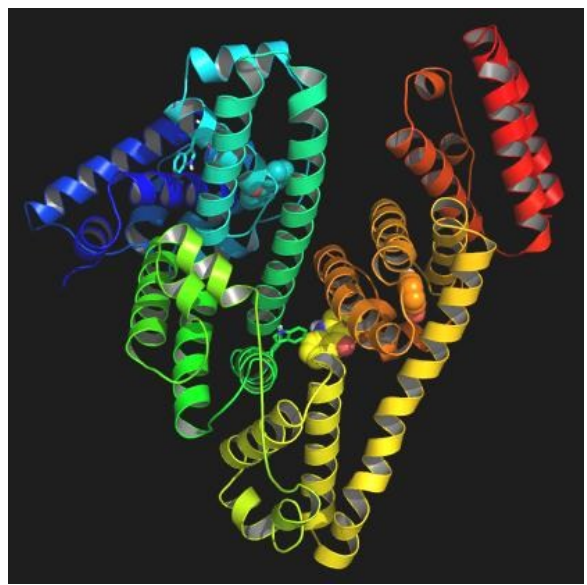
- [1] V.S. Jisha, K.T. Arun, M. Hariharan and D. Ramaiah, *J. Phys. Chem.*, 2010, **114**, 5912.
- [2] I. Vaya, V.L. Vallet, M.C. Jimenez and M.A. Miranda, *Chem. Soc. Rev.*, 2014, **43**, 4102.
- [3] S. Monti and I. Manet, *Chem. Soc. Rev.*, 2014, **43**, 4051.
- [4] B. Chakraborty, A. Singha Roy, S. Dasgupta and S. Basu, *J. Phys. Chem. A*, 2010, **114**, 13313.
- [5] B. Chakraborty, P. Mitra and S. Basu, *RSC Adv.*, 2015, **5**, 81533.
- [6] B. Chakraborty and S. Basu, *J. Lumin.*, 2009, **129**, 34.
- [7] M. Mukherjee, P. Saha Sardar, S.K. Ghorai, S.K. Samanta, A. Singha Roy, S. Dasgupta and S. Ghosh, *PLoS One*, 2013, **8**, e60940.
- [8] N.V. Rakotoarivelo, P. Perio, E. Najahi and F. Nepveu, *J. Phys. Chem. B*, 2014, **118**, 13477.
- [9] H. Liu, W. Bao, H. Ding, J. Jang and G. Zou, *J. Phys. Chem. B*, 2010, **114**, 12938.
- [10] N. Ibrahim, H. Ibrahim, S. Kim, J.P. Nallet and F. Nepveu, *Biomacromolecules*, 2010, **11**, 3341.
- [11] C. Wan, T. Feibig, O. Schiemann, J.K. Barton and A.H. Zewail, *Proc. Natl. Acad. Sci. U.S.A.*, 2000, **97**, 14052.
- [12] I. Vaya, P. Bonancia, M.C. Jimenez, D. Markovitsai, T. Gustavsson and M.A. Miranda, *Phys. Chem. Chem. Phys.*, 2013, **15**, 4727.
- [13] M. Gil, Y. Wang and A. Douhal, *J. Photochem. Photobiol. A*, 2012, **234**, 146.
- [14] Y. Wang, B. Cohen, L. Jicsinszky and A. Douhal, *Langmuir*, 2012, **28**, 4363.
- [15] K. Gavvala, S. Satpathi and P. Hazra, *RSC Adv.*, 2015, **5**, 72793.
- [16] A. Ray, B. Koley Seth, U. Pal and S. Basu, *Spectrochim. Acta Part A*, 2012, **92**, 164.
- [17] M. Banerjee, U. Pal, A. Subuddhi, A. Chakrabarti and S. Basu, *J. Photochem. Photobiol. B*, 2012, **108**, 23.
- [18] P. Mitra, U. Pal, N.C. Maiti, A. Ghosh, A. Bhunia and S. Basu, *RSC Adv.*, 2016, **6**, 53454.
- [19] E.D. Varnell and H.E. Kaufman, *Infect. Immun.*, 1973, **7**, 518.
- [20] C. Fritsch, G. Goerz and T. Ruzicka, *Arch. Dermatol.*, 1998, **134**, 207.
- [21] H. Satonaka, K. Kusuzaki, T. Matsubara, K. Shintani, T. Wakabayashi, T. Nakamura, A. Matsumine and A. Uchida, *Anticancer Res.*, 2007, **27**, 3339.

- [22] R.W. Armstrong, T. Kurucsev and U.P. Strauss, *J. Am. Chem. Soc.*, 1970, **92**, 3174.
- [23] N. Hiashi, M. Takahashi and M. Niwa, *Langmuir*, 1999, **15**, 111.
- [24] H. Baruah, C.S. Day, M.W. Wright and U. Bierbach, *J. Am. Chem. Soc.*, 2004, **126**, 4492.
- [25] Y.J. Hu, H.L. Yue, X.L. Li, S.S. Zhang, E. Tang and L.P. Zhang, *J. Photochem. Photobiol. B*, 2012, **112**, 16.
- [26] F. Foster, *Albumin Structure, Function and Uses*, Pergamon Press, Oxford, UK, 1977.
- [27] S. Patra, K. Santosh, A. Pabbathi and A. Samanta, *RSC Adv.*, 2012, **2**, 6079.
- [28] (a) G. Sudlow, D. J. Birkett and D. N. Wade, *Mol. Pharmacol.*, 1975, **11**, 824.
- [29] M. Hossain, A.Y. Khan and G.S. Kumar, *PLoS One*, 2011, **6**, e18333.
- [30] A. S. R. Koti, M. M. G. Krishna and N. Periasamy, *J. Phys. Chem. A*, 2001, **105**, 1767.
- [31] A. S. R. Koti and N. Periasamy, *J. Chem. Phys.*, 2001, **115**, 7094.
- [32] M. Maroncelli and G. R. Fleming, *J. Chem. Phys.*, 1987, **86**, 6221.
- [33] F. Moreno, M. Cortijo and J.G. Jimenez, *Photochem. Photobiol.* 1999, **70**, 695.
- [34] J.R. Lakowicz, *Principles of Fluorescence Spectroscopy*, Plenum Press, New York, 2006.
- [35] G.M. Morris, R. Huey, W. Lindstrom, M.F. Sanner, R.K. Belew, D.S. Goodsell and A.J. Olson, *J. Comput. Chem.*, 2009, **30**, 2785.
- [36] K.A. Majorek, P.J. Porebski, A. Dayal, M.D. Zimmerman, K. Jablonska, A.J. Stewart, M. Chruszcz, and W. Minor, *Mol. Immunol.*, 2012, **52**, 174.
- [37] M.D. Hanwell, D.E. Curtis, D.C. Lonie, T. Vandermeersch, E. Zurek and G.R. Hutchison, *J. Cheminformatics*, 2012, **4**, 17.
- [38] M. Gerstein, *Acta Crystallogr. A*, 1992, **48**, 271.
- [39] A. Singha Roy, D.R. Tripathy, A. Chatterjee and S. Dasgupta, *J. Biophys. Chem.*, 2010, **1**, 141.
- [40] J. Wang, L. Ma, Y. Zhang and T. Jiang, *J. Mol. Struct.*, 2017, **1129**, 160.
- [41] B.K. Paul, D. Ray and N. Guchhait, *Phys. Chem. Chem. Phys.*, 2012, **14**, 8892.
- [42] S. Dasmandal, A. Kundu, S. Rudra and A. Mahapatra, *RSC Adv.*, 2015, **5**, 79107.
- [43] S. M. Kelly and N. C. Price, *Curr. Protein Pept. Sci.*, 2000, **1**, 349.
- [44] M. Amina, M.A. Ali, N.M. Al-Musayeib and H.A. Al-Lohedan, *J. Mol. Liq.*, 2016, **220**, 931.
- [45] T. Asakura, K. Adachi and E. Schwartz, *J. Biol. Chem.*, 1978, **253**, 6423.

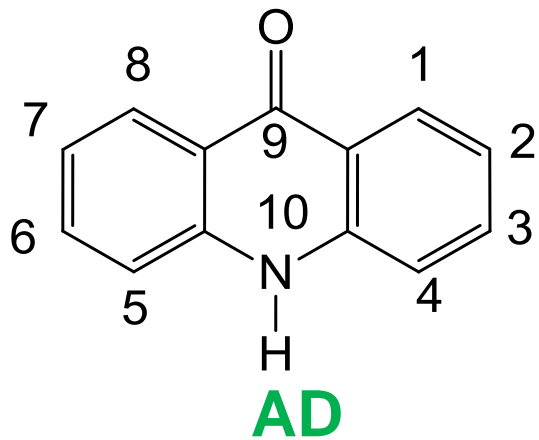
- [46] M. Bardhan, T. Misra and T. Ganguly, *J. Photochem. Photobiol. B*, 2012, **106**, 113.
- [47] X. He and D. C. Carter, *Nature*, 1992, **358**, 209.
- [48] M.R. Eftink and C.A. Ghiron, *Biochemistry*, 1977, **16**, 5546.
- [49] S. Patel and A. Datta, *J. Phys. Chem. B*, 2007, **111**, 10557.
- [50] N. Zhou, Y.Z. Liang and P. Wang, *J. Photochem. Photobiol. A*, 2007, **185**, 271.
- [51] C.X. Wang, F.F. Yan, Y.X. Zhang and L. Ye, *J. Photochem. Photobiol. A*, 2007, **192**, 23.
- [52] A. Barik, B. Mishra, A. Kunwar and K. I. Priyadarsini, *Chem. Phys. Lett.*, 2007, **436**, 239.
- [53] U. Anand, C. Jash, R.K. Boddepalli, A. Shrivastava and S. Mukherjee, 2011, *J. Phys. Chem. B*, **115**, 6312.
- [54] B.K. Paul, A. Samanta and N. Guchhait, *J. Phys. Chem. B*, 2010, **114**, 6183.
- [55] N.S. Moyon, M.M. Islam, S. Phukan and S. Mitra, *J. Photochem. Photobiol. B*, 2013, **121**, 37.
- [56] X. Li and Y. Hao, *J. Mol. Struct.*, 2015, **1091**, 109.
- [57] T. Wang, Z. Zhao, B. Wei, L. Zhang and L. Ji, *J. Mol. Struct.*, 2010, **970**, 128.
- [58] X. Li and S. Wang, *New J. Chem.*, 2015, **39**, 386.
- [59] B. Ojha and G. Das, *J. Phys. Chem. B*, 2010, **114**, 3979.
- [60] J. Weber and A.E. Senior, *Biochemistry*, 2000, **39**, 5287.
- [61] T.A. Wells, M. Nakazwa, K. Manabe and P.S. Song, *Biochemistry*, 1994, **33**, 708.
- [62] B.K. Paul and N. Guchhait, *J. Phys. Chem. B*, 2011, **115**, 10322.
- [63] B.K. Paul, N. Ghosh and S. Mukherjee, *RSC Adv.*, 2016, **6**, 9984.
- [64] E.L. Quitevis, A.H. Marcus and M.D. Fayer, *J. Phys. Chem.*, 1993, **97**, 5762.
- [65] G. Jia, Z. Feng, C. Wei, J. Zhou, X. Wang and C. Li, *J. Phys. Chem. B*, 2009, **113**, 16237.
- [66] K. Sahu, S.K. Mondal, S. Ghosh, D. Roy and K. Bhattacharyya, *J. Chem. Phys.*, 2006, **124**, 124909.
- [67] A. Chakraborty, D. Seth, P. Setua and N. Sarkar, *J. Chem. Phys.*, 2008, **128**, 204510.
- [68] K. Kinoshita, S. Kawato and A. Ikegami, *Biophys. J.*, 1977, **20**, 289.
- [69] B. Ahmad, S. Parveen and R. H. Khan, *Biomacromolecules*, 2006, **7**, 1350.

- [70] P. D. Ross and S. Subhramanian, *Biochemistry*, 1981, **20**, 3096.
- [71] Y. Akdogan, J. Reichenwallner and D. Hinderberger, *PLoS One*, 2012, **7**, e45681.
- [72] S. Banerjee, S. Dutta Choudhury, S. Dasgupta and S. Basu, *J. Lumin.*, 2008, **128**, 437.
- [73] D. V. Bent and E. Hayon, *J. Am. Chem. Soc.*, 1975, **97**, 2612.
- [74] D. Creed, *Photochem. Photobiol.*, 1984, **39**, 537.
- [75] B. Chakraborty and S. Basu, *Appl. Magn. Reson.*, 2012, **42**, 5.
- [76] D. Das and D. N. Nath, *J. Phys. Chem. A*, 2008, **112**, 11619.
- [77] S. Dutta Choudhury and S. Basu, *J. Phys. Chem. B*, 2006, **110**, 8850.
- [78] S. Sheth, A. Baron, C. Herrero, B. Vauzeilles, A. Aukauloo and W. Leibl, *Photochem. Photobiol. Sci.*, 2013, **12**, 1074.
- [79] S. Curry, H. Mandelkow, P. Brick and N. Franks, *Nat. Struct. Biol.*, 1998, **5**, 827.
- [80] J. Reichenwallner and D. Hinderberger, *Biochim. Biophys. Acta BBA - Gen. Subj.*, 2013, **1830**, 5382.
- [81] J.R. Simard, P.A. Zunszain, J.A. Hamilton and S. Curry, *J. Mol. Biol.*, 2006, **361**, 336.

AD initially gets hooked to Trp 212 housed in domain IIA, inducing conformational changes in the protein and paving way for the ligand to reach Trp 134 located in domain IB.



BSA



AD

